Electronic Supplementary Material (ESI) for Journal of Materials Chemistry A.

Electronic Supplementary Information

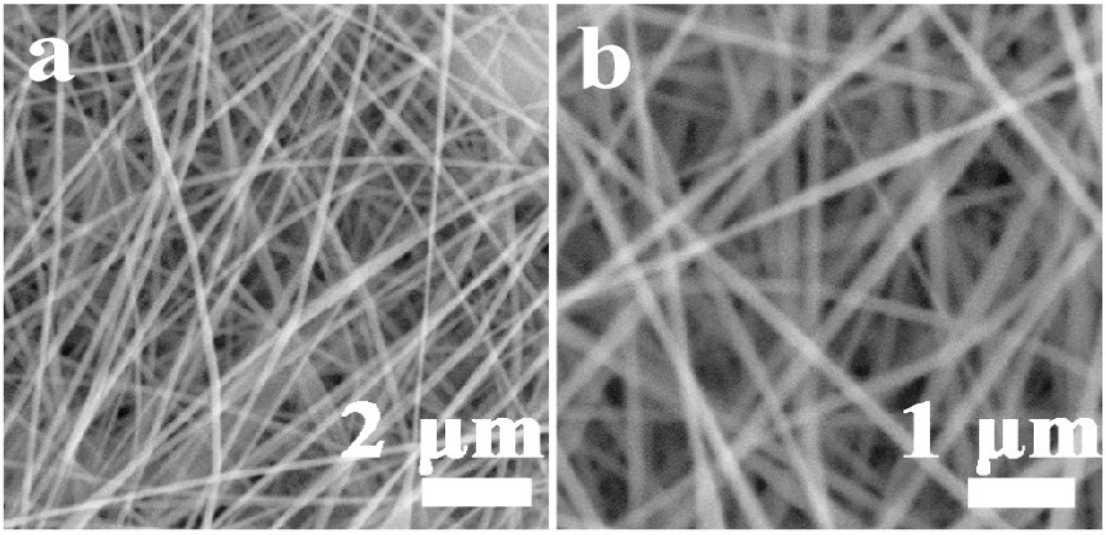

Fig. S1 (a, b) SEM images of PAN nanofibers.

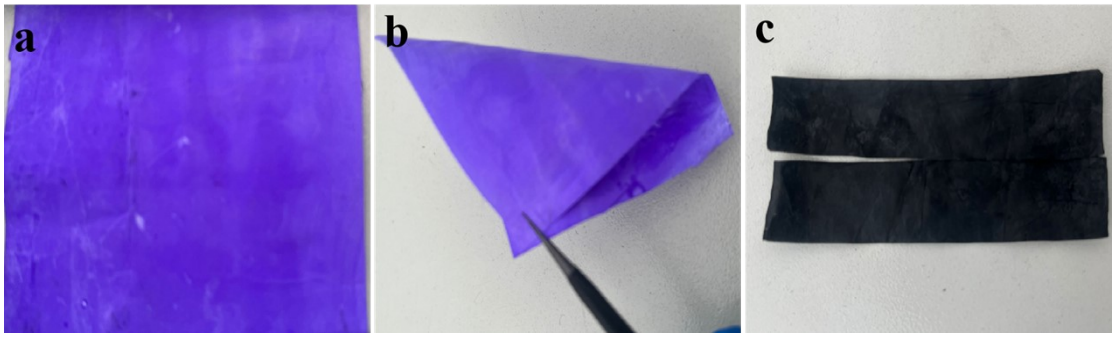

Fig. S2 Digital photos of the flexible film: (a, b) PAN@ZIF-67 nanofibers, (c) CNF@Co@C composites.

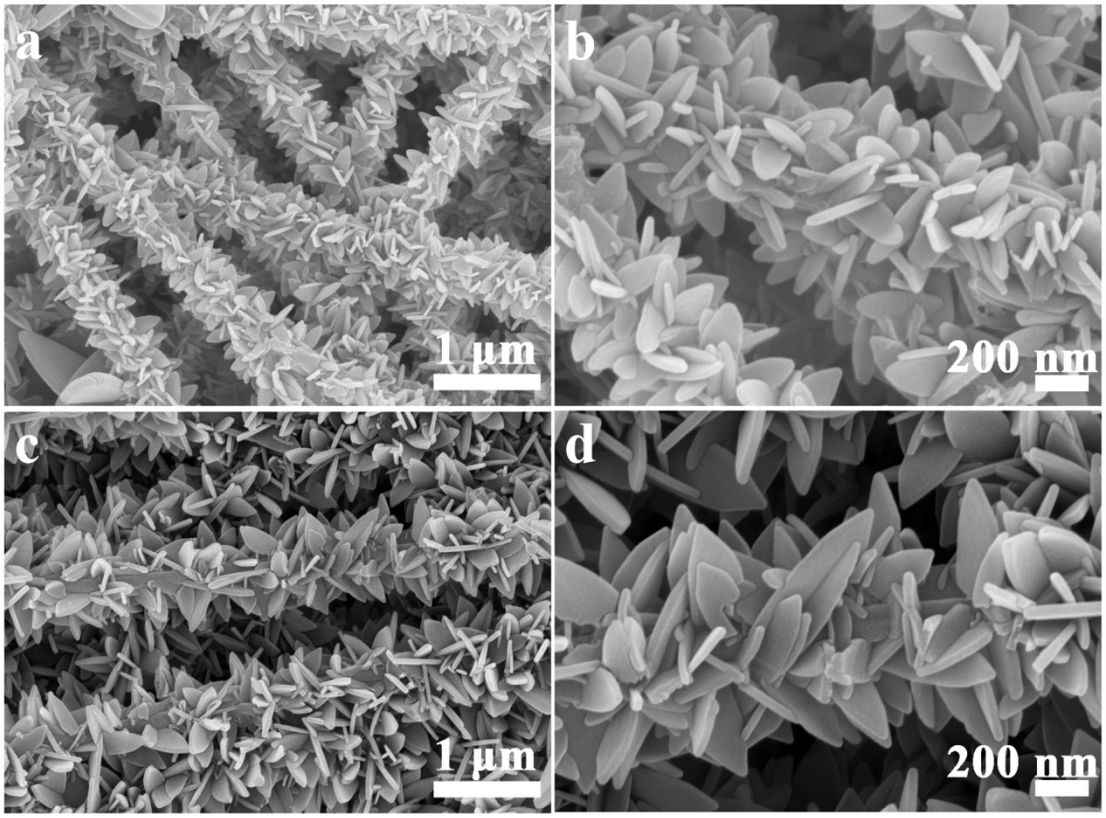

Fig. S3 SEM images of the PAN@ZIF-67/ZIF-8 nanofibers (a, b) and PAN@ZIF-8 nanofibers (c, d).

Note: PAN@ZIF-67/ZIF-8 nanofibers were synthesized as well through same procedure of the PAN@ZIF-67 nanofibers but using 1 mmol $Co(NO_3)_2.6H_2O$ and 1 mmol $Zn(NO_3)_2.6H_2O$ dissolved in 20 deionized water, meanwhile, 1.3 g 2-MIM was dissolved into 20 ml deionized water as well. In addition, PAN@ZIF-67/ZIF-8 nanofibers were synthesized as well through same procedure of the PAN@ZIF-67 nanofibers but using 2 mmol $Zn(NO_3)_2.6H_2O$ dissolved in 20 deionized water, meanwhile, 1.3 g 2-MIM was dissolved into 20 ml deionized water as well.

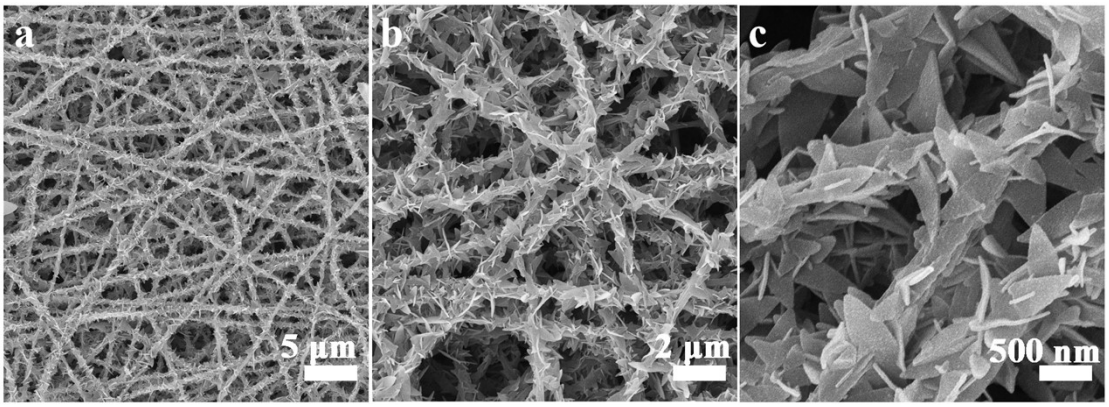

Fig. S4 (a-c) SEM images of the CNF@Co@C composites.

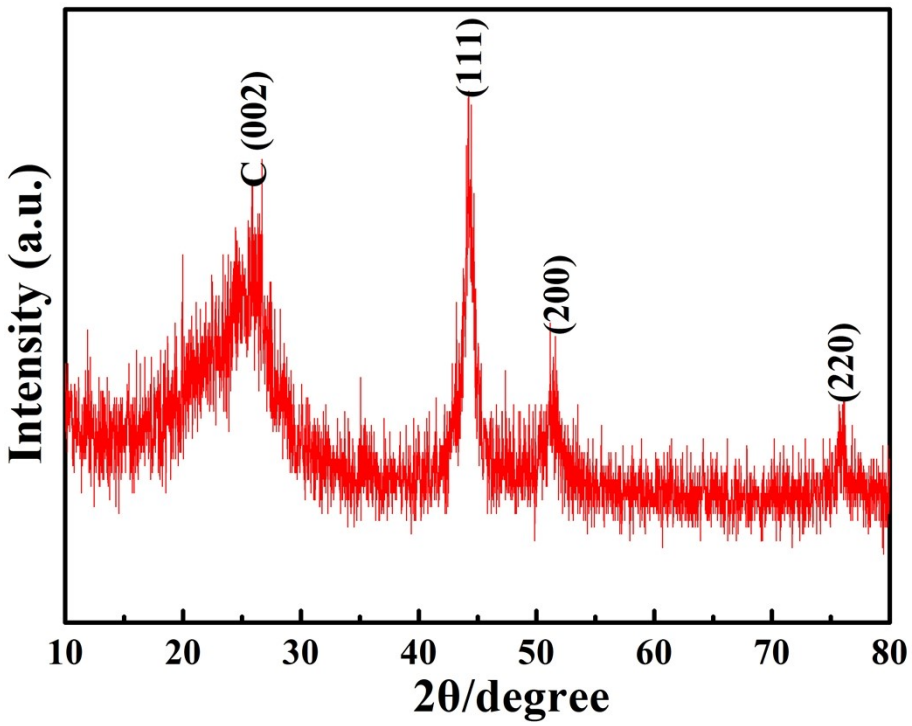

Fig. S5 XRD pattern of the CNF@Co@C composites.

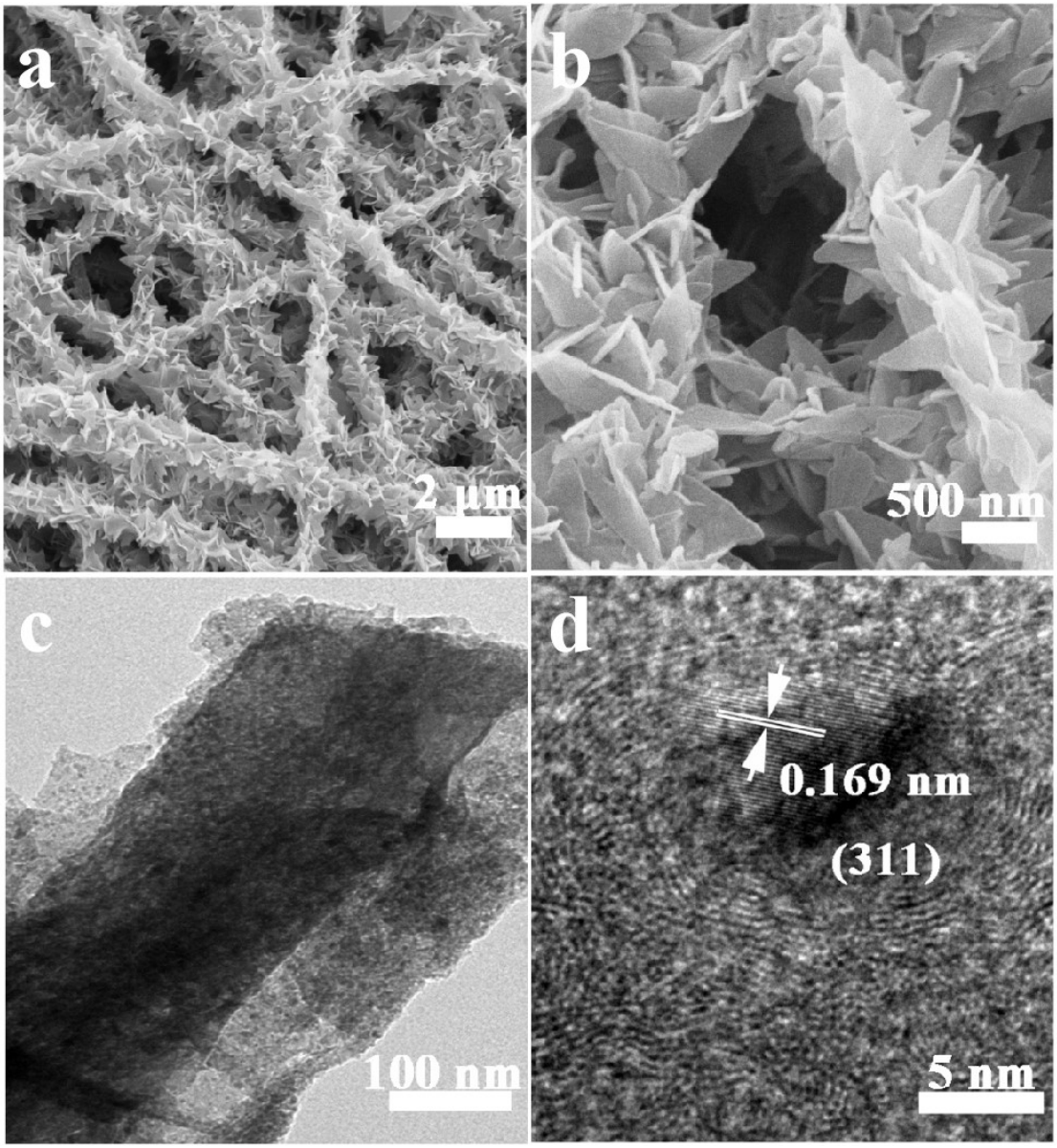

Fig. S6 (a, b) SEM images of the CNF@CoS_2@C composites, TEM (c) and HRTEM (d) images of the CNF@CoS_2@C composites.

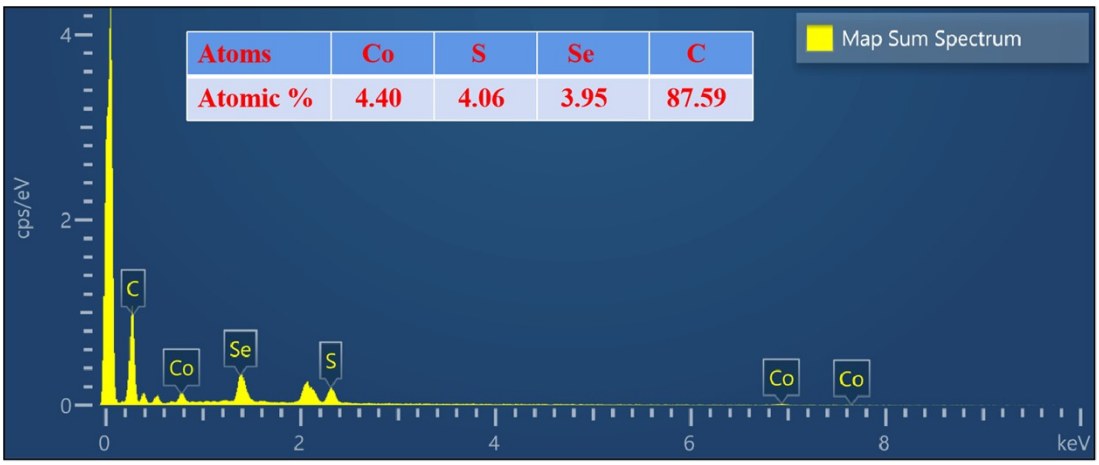

Fig. S7 EDX spectrum of the CNF@CoSSe@C composites.

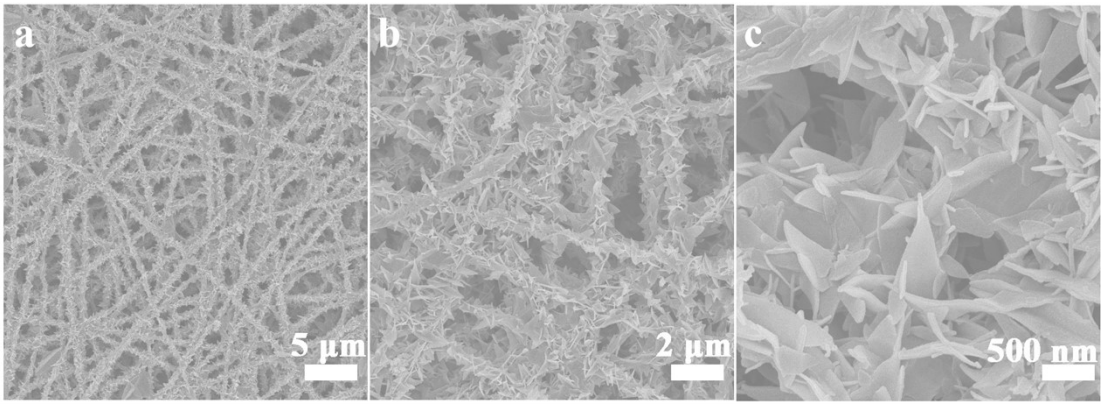

Fig. S8 SEM image of the CNF@$CoSe_2$@C composites.

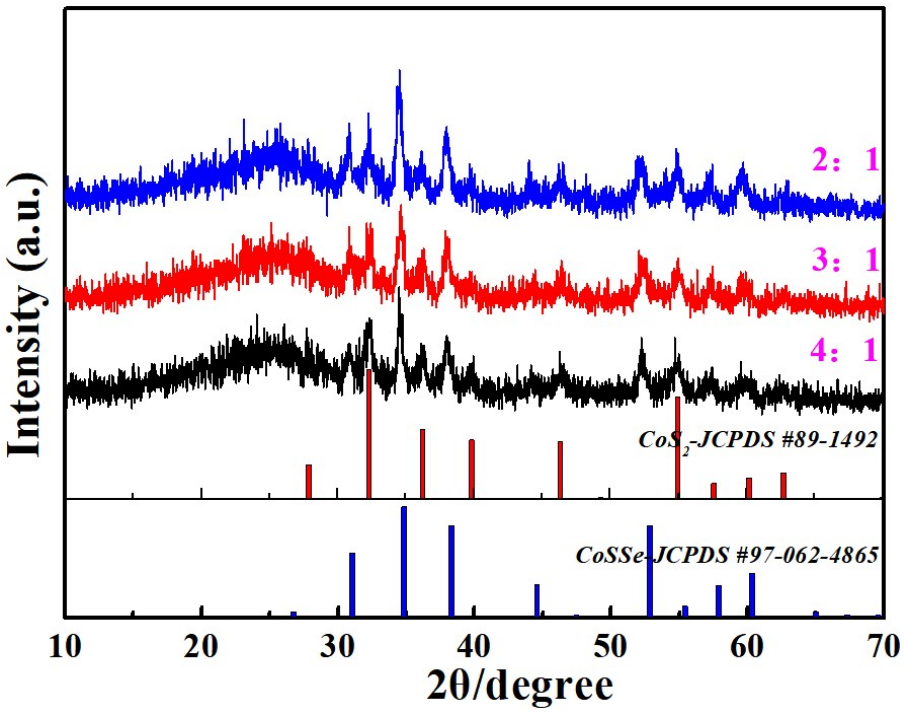

Fig. S9 XRD patterns of the CoSSe@C cmposites at different mass ratio between CNF@CoS_2@C and Se powder.

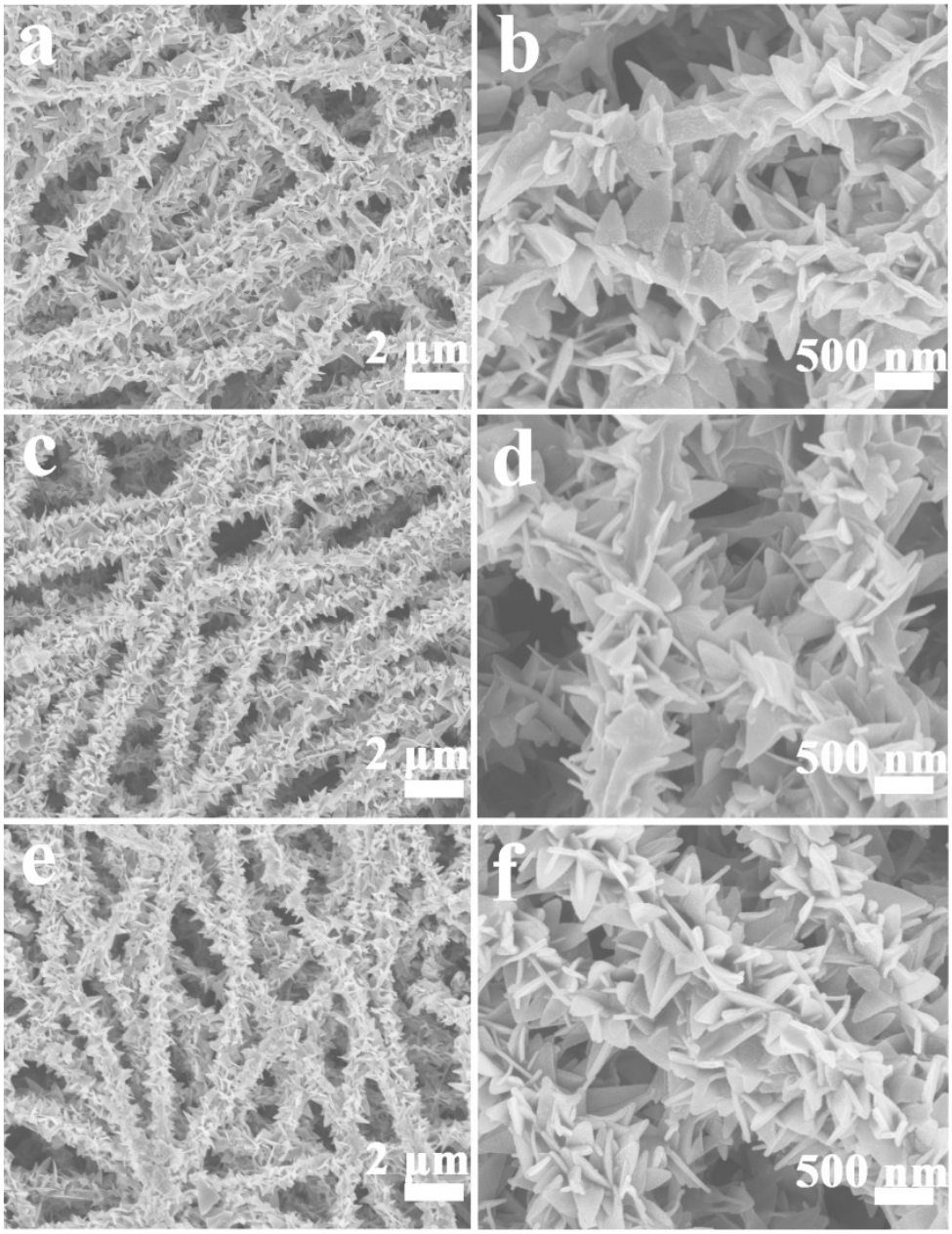

Fig. S10 SEM images of the CoSSe@C composites at different mass ratios between CNF@CoS_2@C and Se powder : (a, b) 2:1; (c, b) 3:1; (e, f) 4:1.

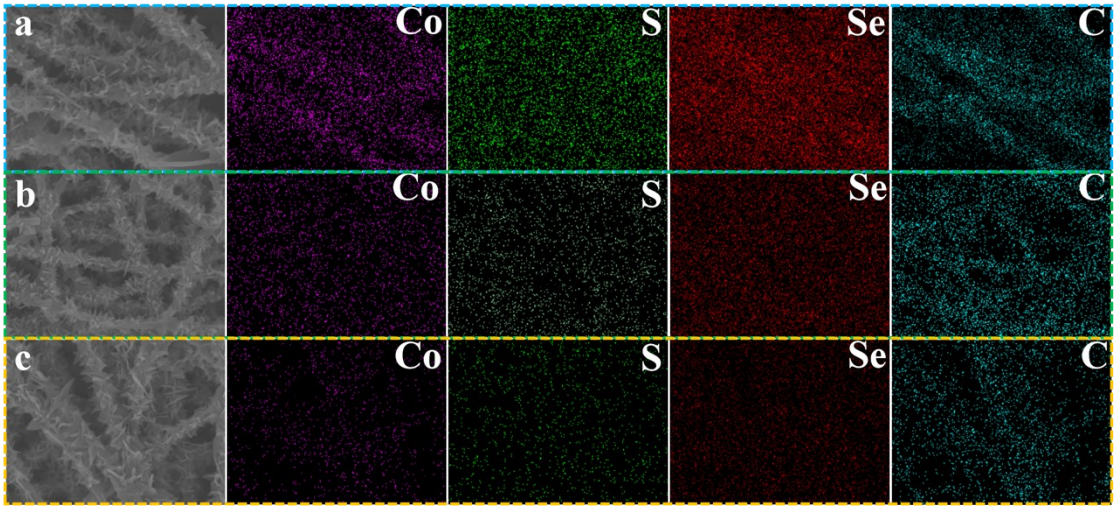

Fig. S11 EDX elemental mapping images of the CoSSe@C composites at different mass ratio between CNF@CoS_2@C and Se powder: (a, b) 2:1; (c, b) 3:1; (e, f) 4:1.

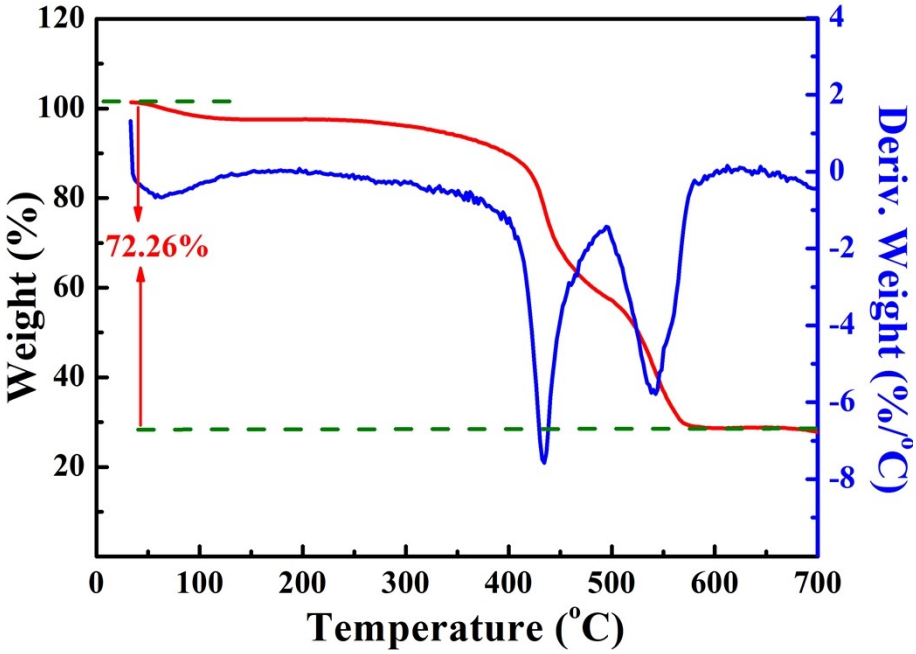

Fig. S12 TGA curves of the CNF@CoSSe@C composites.

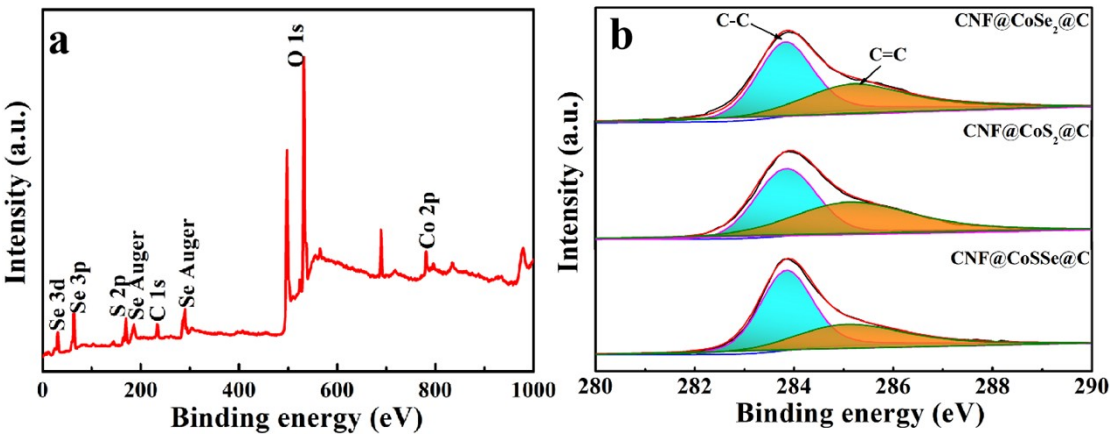

Fig. S13 (a) XPS survey spectrua of the CNF@CoSSe@C composites, (b) high-resolution C 1s spectra of the CNF@CoSSe@C, CNF@CoS_2@C, CNF@$CoSe_2$@C composites.

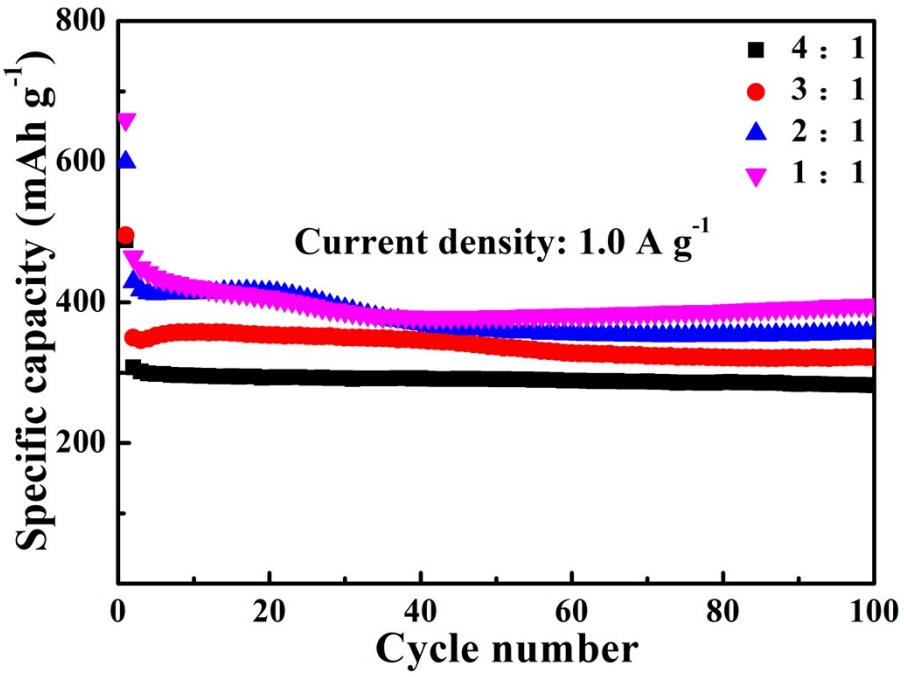

Fig. S14 Electrochemical performance of the CoSSe@C cmposites at different mass ratio between CNF@CoS_2@C and Se powder.

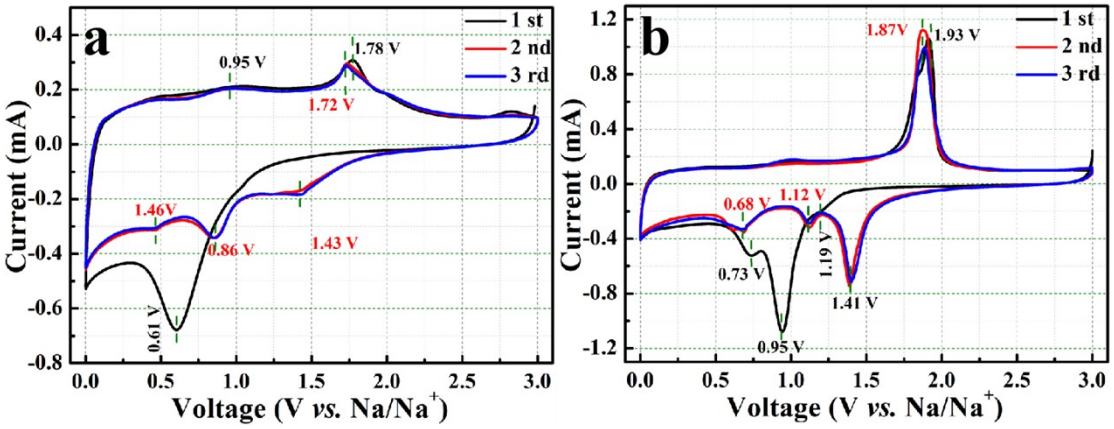

Fig. S15 CV profiles of the electrodes at 0.5 mV s^{-1}: (a) CNF@CoS_2@C, (b) CNF@$CoSe_2$@C.

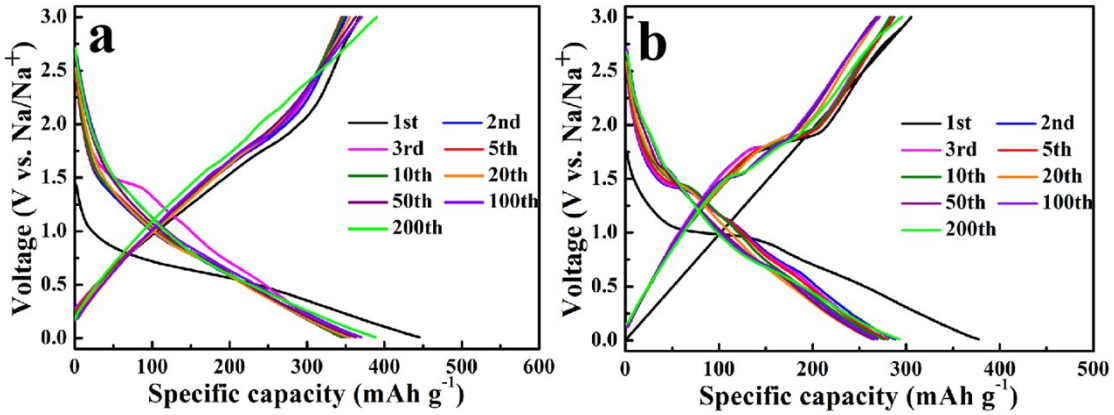

Fig. S16 GCD profiles of the electrodes at 1.0 A g^{-1}: (a) CNF@CoS_2@C, (b) CNF@$CoSe_2$@C.

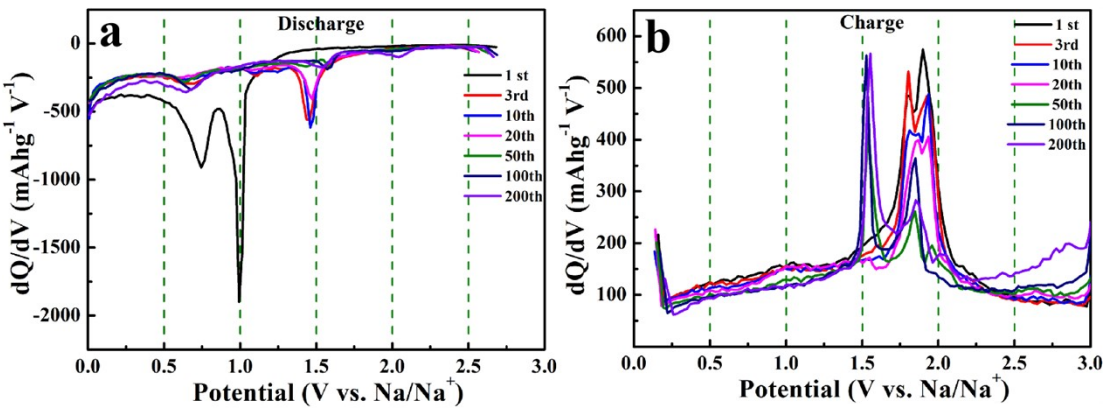

Fig. S17 The differential capacity curves of the CNF@CoSSe@C electrode at 1.0 A g^{-1}.

Note: In Fig. S17a, two obvious cathodic peaks located at about 0.98 and 0.74 V agree with the CV results. As the cycle continues from 2 nd to 20 th cycle, a peak at about 1.47 V disappeared and meanwhile two new peaks at about 1.57 and 2.04 V were found. During the charging process from 1st to 20th cycle (Fig. S17b), the peaks at about 1.82 and 1.91 V are due to the stepwise desodiation process generating the single CoSSe or mixed CoS and CoSe structure. From 50th to 200 th cycle, an obvious anodic peak at 1.55 V appears. The appearance and transfer of these new redox peaks maybe raised by the continuous activation behaviors of the electrode material during the repeated Na^+ de-intercalation.

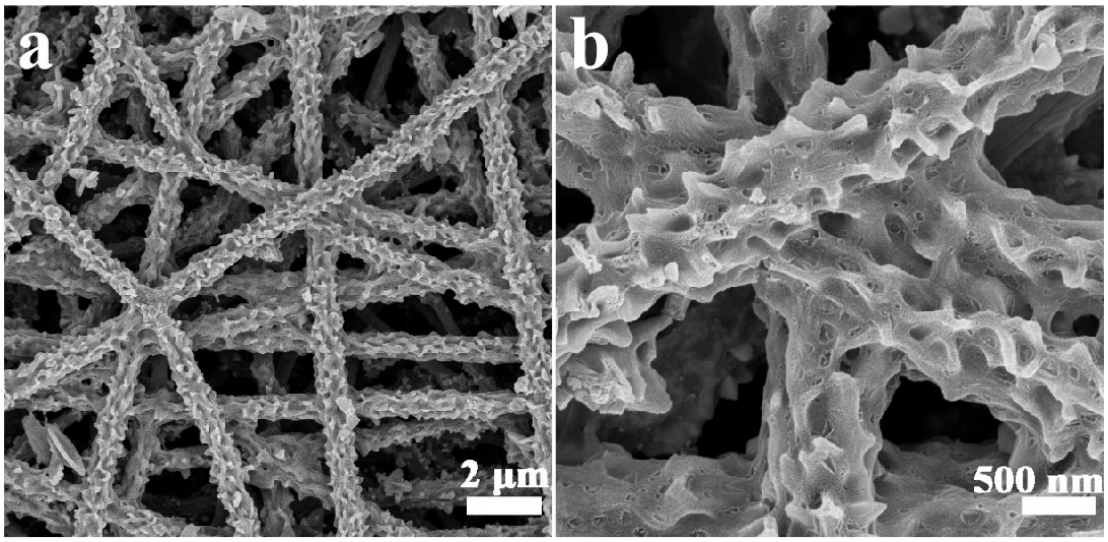

Fig. S18 SEM images for the CNF@CoSSe@C film as binder-free anode after cycling.

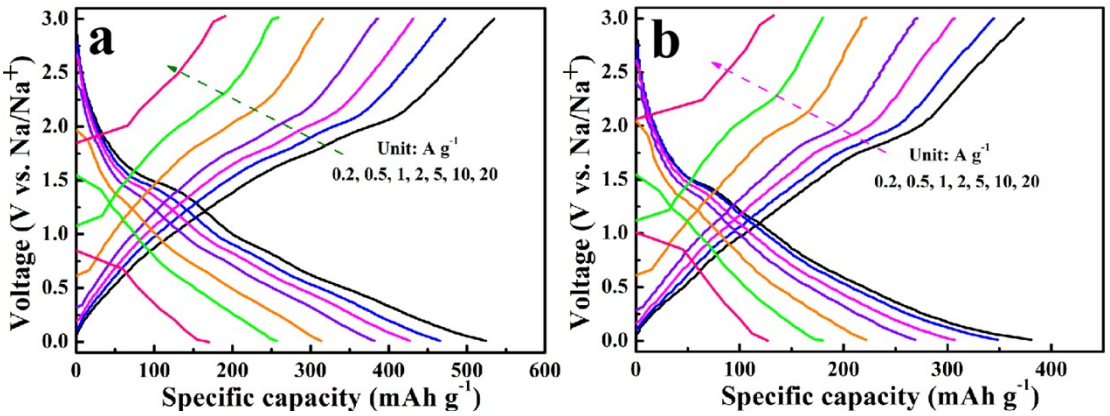

Fig. S19 GCD profiles of the electrodes at different rates: (a) CNF@CoS_2@C, (b) CNF@$CoSe_2$@C.

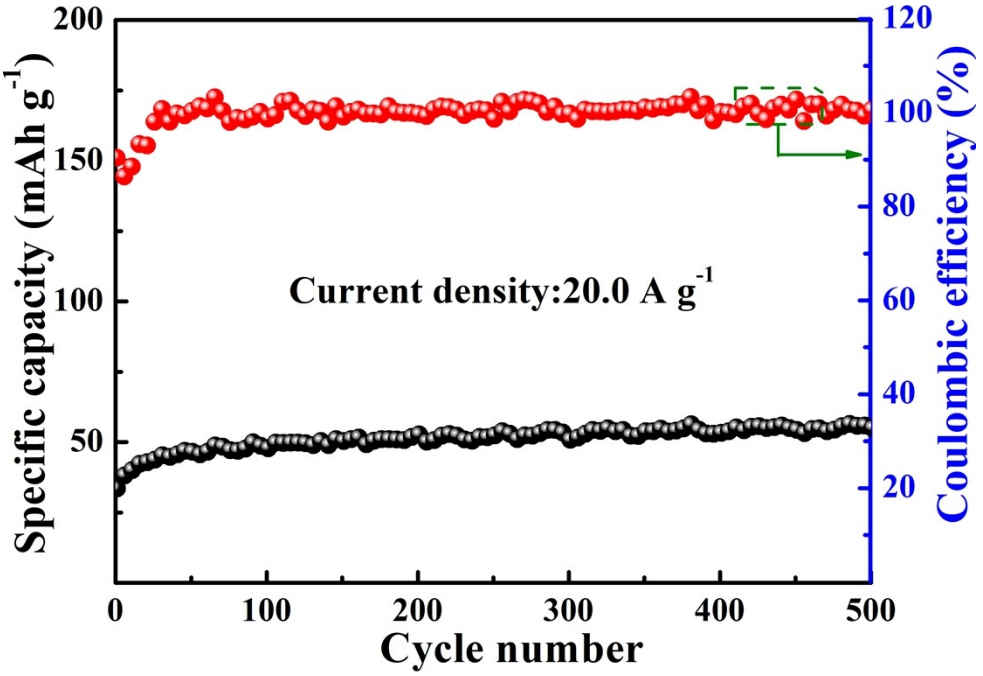

Fig. S20 The cycling performance of the pure carbon at 20.0 A g^{-1} with a voltage window of 0.01-3.0V.

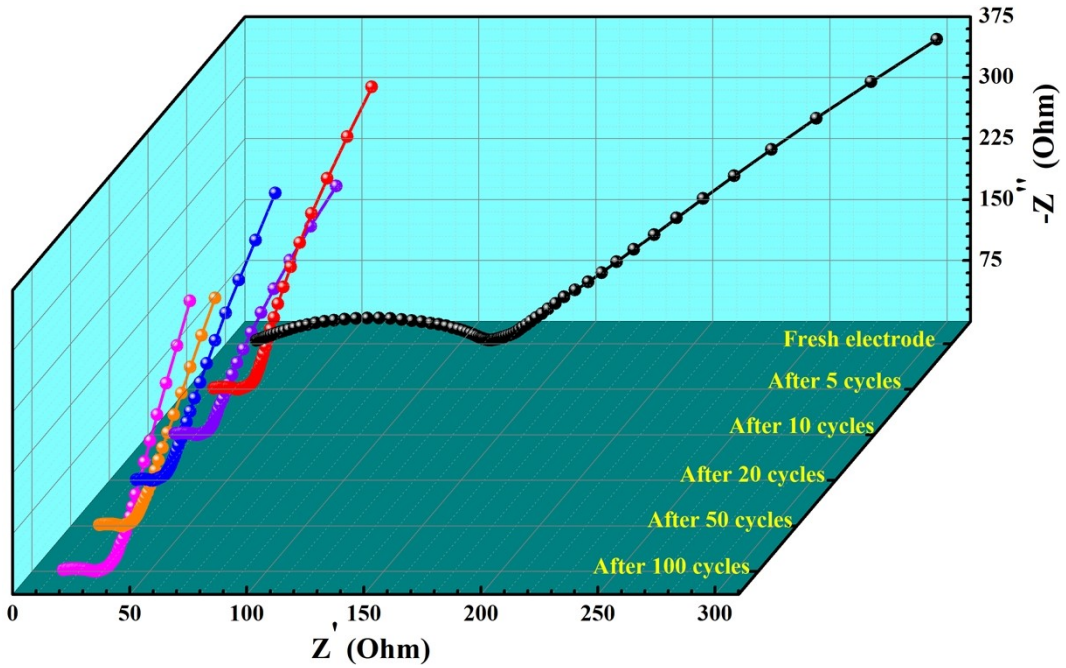

Fig. S21 In-situ Nyquist plots of the CNF@CoSSe@C composites at predetermined cycles.

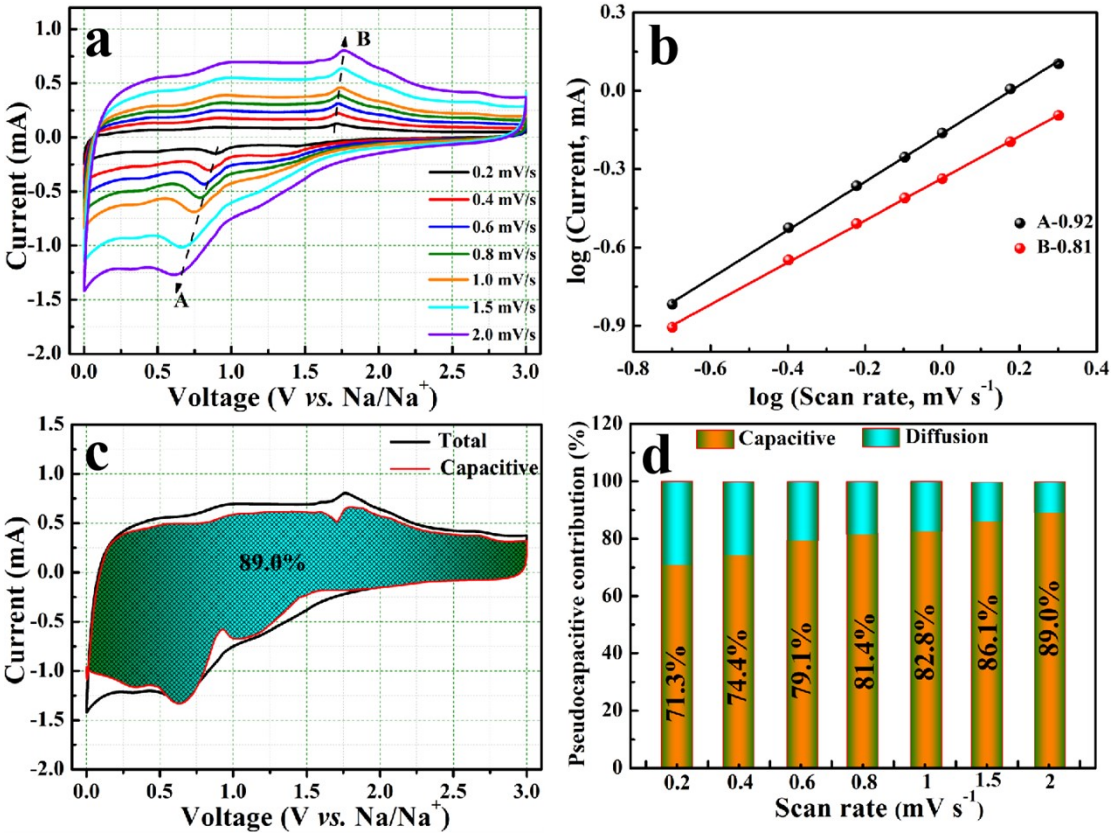

Fig. S22 Scan rate-dependent CV curves (a), the plots of log*i* and log*v* at each redox peak (b), capacitive charge contribution (dark green shadow) at 2.0 mV s^{-1} (c), and the normalized percentage of capacitive contributions at distinct scan rates (d) for the CNF@CoS_2@C electrode.

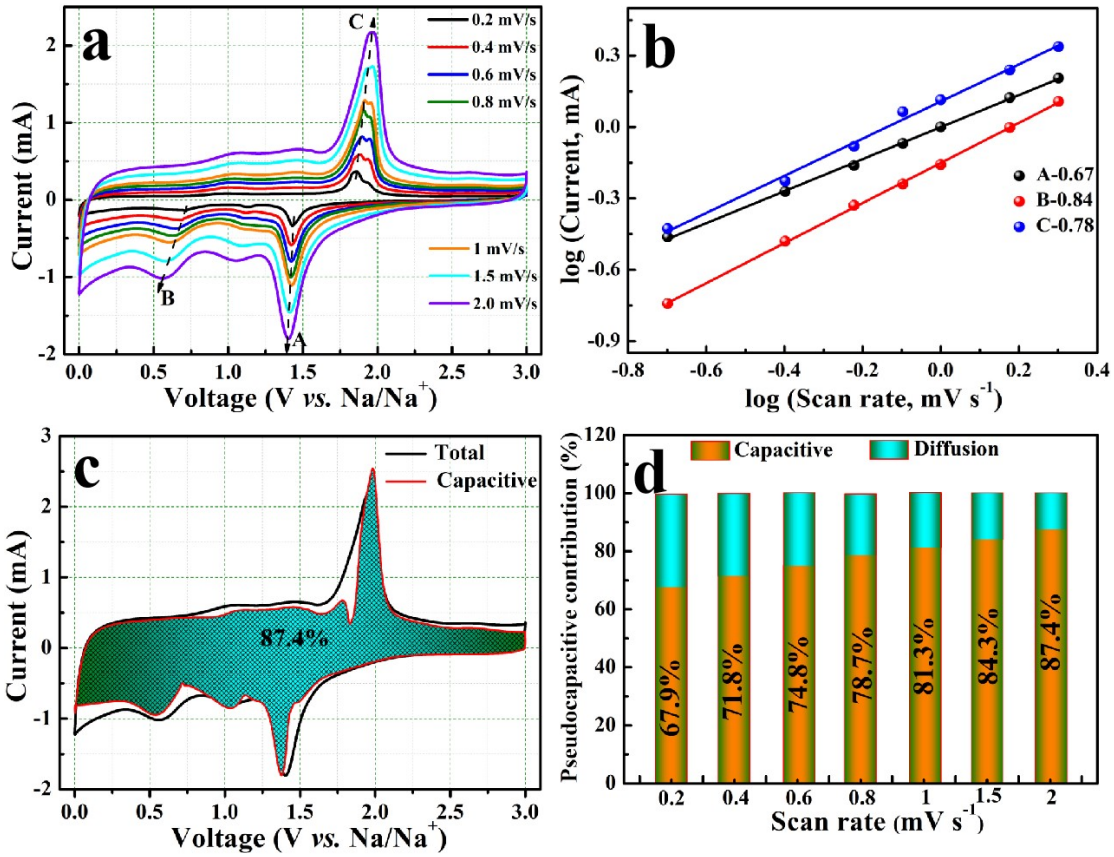

Fig. S23 Scan rate-dependent CV curves (a), the plots of log*i* and log*v* at each redox peak (b), capacitive charge contribution (dark green shadow) at 2.0 mV s^{-1} (c), and the normalized percentage of capacitive contributions at distinct scan rates (d) for the CNF@$CoSe_2$@C electrode.

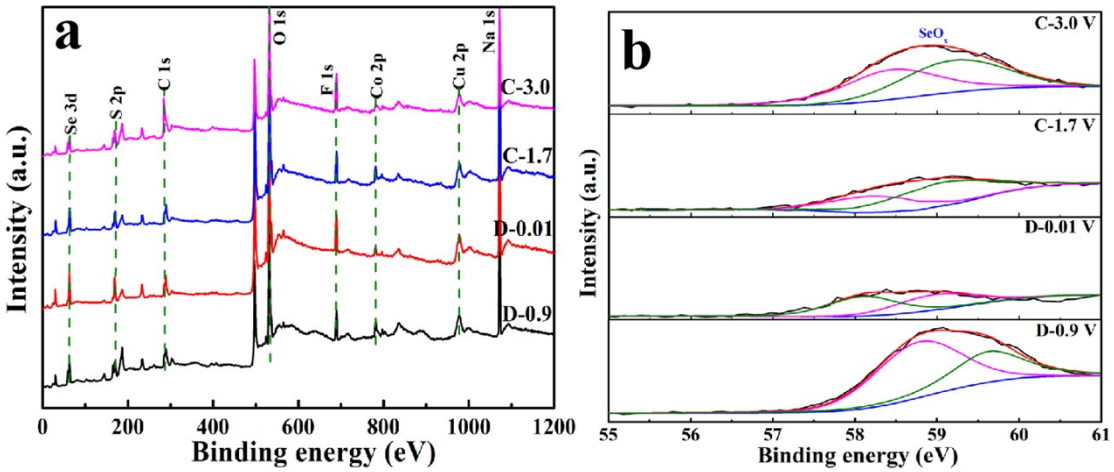

Fig. S24 Ex-situ XPS spectra of the CNF@CoSSe@C electrode at predetermined voltage states: (a) XPS Survey spectra; (b) High-resolution C 1s spectra.

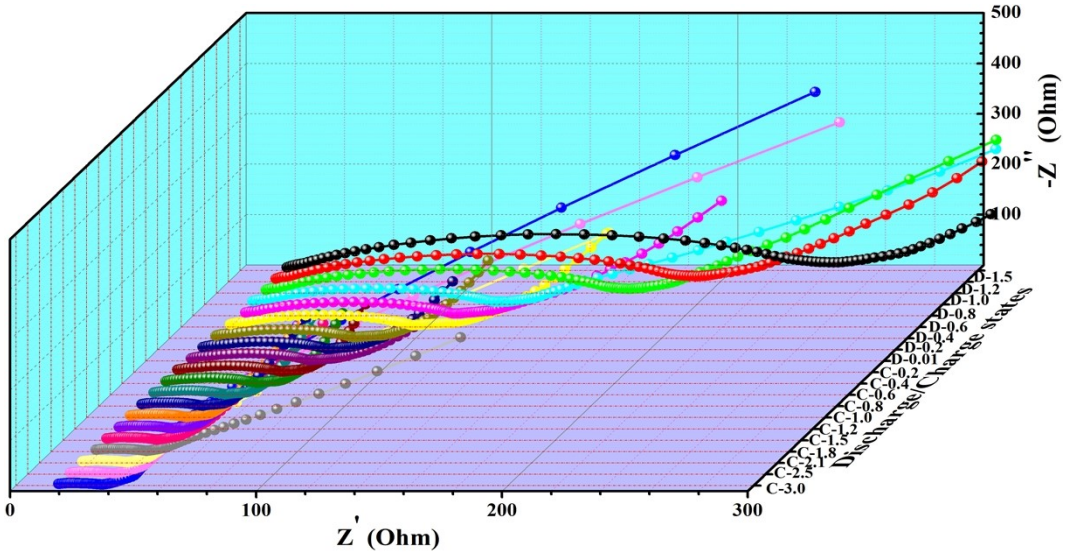

Fig. S25 In-situ Nyquist plots of the CNF@CoSSe@C composites with respect to predetermined potentials within the 1st cycle.

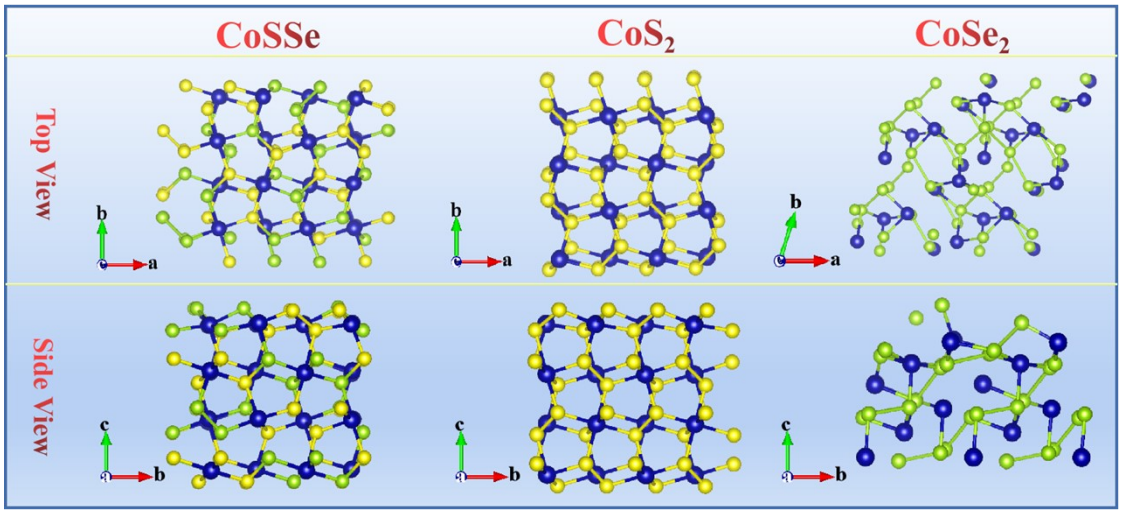

Fig. S26 The surface slab models of the CoSSe, CoS_2, and $CoSe_2$.

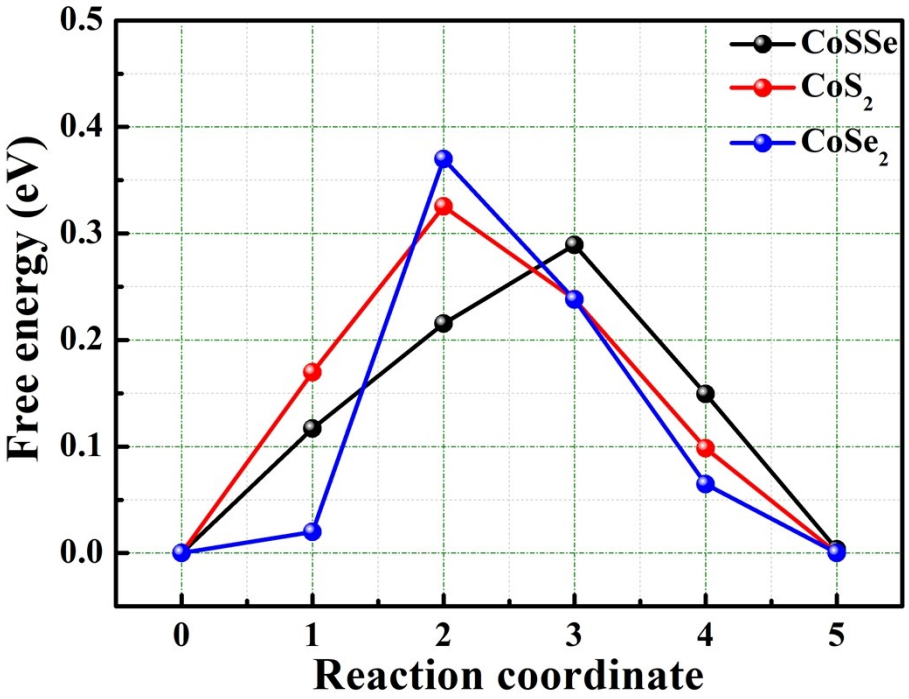

Fig. S27 The Na^+ migration energy barriers of the CoSSe, CoS_2 and $CoSe_2$ models.

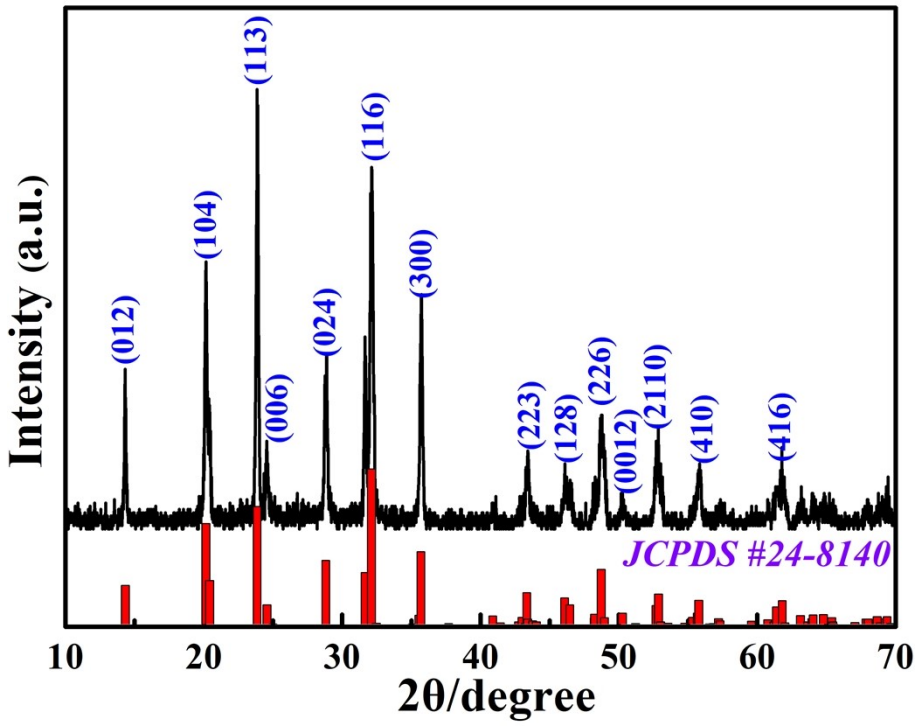

Fig. S28 XRD pattern of the NVP@C.

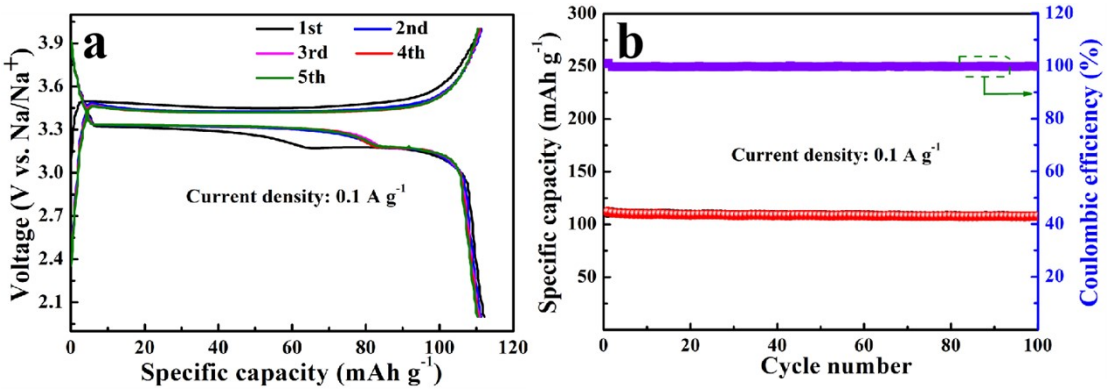

Fig. S29 GCD profiles (a) and cycling performance (b) of the NVP@C cathode at 0.1 A g^{-1}.

Table S1 Comparison of cycle lifespan and specific capacity of the CNF@CoSSe@C with previous reported CoS_2- and $CoSe_2$-based anodes in SIBs systems.

Materials	Voltage window (V)	Rate (A g^{-1})	Cycle number	Capacity (mAh g^{-1})	Ref.
Cu-$CoSe_2$ microboxes	0.01-3.0	1.0	500	374.0	1
$CoSe_2$@NC@TiO_2	0.01-3.0	0.2	200	374.0	2
$CoSe_2$@CNF	0.01-3.0	2.0	1000	370.0	3
$CoSe_2$/WSe_2@@C/CNs	0.01-3.0	0.5	200	277.0	4
P-$CoSe_2$/C	0.01-3.0	0.2	200	322.0	5
Multishell $CoSe_2$	0.01-3.0	1.0	2000	319.0	6
N-CNT/rGO/$CoSe_2$	0.3-2.9	10.0	10000	264.0	7
Hollow microflower-like $CoSe_2$	0.5-3.0	1.0	1690	220.0	8
CoS_2/Sb_2S_3@NC/CNT	0.01-3.0	0.5	200	360.1	9
rGO-CoS_2-GNCSs	0.4-2.9	1.0	400	412.3	10
f-Ti_3C_2/CoS_2@NPC	0.01-3.0	10.0	8000	104.1	11
AGC-CoS_2/NCNFs	0.01-3.0	3.2	1000	148.0	12
SnS_2-CoS_2@C	0.2-3.0	5.0	500	402.5	13
Cu-CoS_2@CuxS	0.4-2.6	0.3	300	385.0	14
CoS_2@MCNFs	0.4-2.9	1.0	900	620.0	15
CNF@CoSSe@C	**0.01-3.0**	**20.0**	**13000**	**158.2**	**This work**

References

1 Y. J. Fang, X. Y. Yu and X. W. Lou, *Adv. Mater.,* 2018, **21**, 1706668.

2 B. Zhao, Q. Q. Liu, G. J. Wei, J. H. Wang, X. Y. Yu, X. Li and H. B. Wu, *Chem. Eng. J.*, 2019, **378**, 122206.

3 H. Yin, H. Q. Qu, Z. T. Liu, R. Z. Jiang, C. Li and M. Q. Zhu, *Nano Energy*, 2019, **58**, 715−723.

4 S. Q. Zhang, L. L. Sun, L. Yu, G. H. Zhai, L. X. Li, X. J. Liu and H. Wang, *Small*, 2021, **49**, 2103005.

5 J. J. Ye, X. T. Li, G. Xia, G. H. Gong, Z. Q. Zheng, C. Z. Chen and C. Hu, *J. Mater. Sci. Technol.*, 2021, **77**, 100−107.

6 H. J. Liang, X. T. Li, X. L. Liu, R. Sun, Z. X. Qin, Y. F. Zhang and H. S. Fan, *J. Power Sources*, 2022, **517**, 230729.

7 M. S. Jo, J. S. Lee, S. Y. Jeong, J. K. Kim, Y. C. Kang, D. W. Kang, S. M. Jeong and J. S. Cho, *Small*, 2020, **38**, 2003391.

8 X. Q. Ma, L. Zou and W. X. Zhao, *Chem. Commun.*, 2018, **54**, 10507−10510.

9 X. T. Li, H. J. Liang, X. L. Liu, R. Sun, Z. X. Qin, H. S. Fan and Y. F. Zhang, *Chem. Eng. J.*, 2021, **425**, 130657.

10 X. He, L. N. Bi, Y. Li, C. G. Xu and D. M. Lin, *Electrochim. Acta*, 2020, **332**, 135453.

11 P. F. Huang, H. J. Ying, S. L. Zhang, Z. Zhang and W. Q. Han, *Chem. Eng. J.*, 2022, **429**, 132396.

12 W. M. Zhang, Z. W. Yue, Q. M. Wang, X. X. Zeng, C. C. Fu, Q. Li, X. T. Li, L. D. Fang and L. Li, *Chem. Eng. J.*, 2020, **380**, 122548.

13 X. Q. Liu, Y. Xiang, Q. P. Li, Q. J. Zheng, N. Jiang, Y. Huo and D. M. Lin, *Electrochim. Acta*, 2021, **387**, 138525.

14 Y. J. Fang, D. Y. Luan, Y. Chen, S. Y. Gao and X. W. Lou, *Angew. Chem. Int. Ed.,* 2020, **7**, 2644−2648.

15 Y. L. Pan, X. D. Cheng, L. L. Gong, L. Shi, T. Zhou, Y. R. Deng and H. P. Zhang, *ACS Appl. Mater. Interfaces*, 2018, **10**, 31441−31451.